Chapter

Turbulent Heat Transfer Analysis of Silicon Carbide Ceramic Foam as a Solar Volumetric Receiver

Chen Yang, Huijin Xu and Akira Nakayama

Abstract

A volumetric solar receiver receives the concentrated radiation generated by a large number of heliostats. Turbulent heat transfer occurs from the solid matrix to the air as it passes through the porous receiver. Such combined heat transfer within the receiver, including radiation, convection and conduction, is studied using a local thermal non-equilibrium model. Both the Rosseland approximation and the P1 model are applied to consider the radiative heat transfer through the solar receiver. Furthermore, the low Mach approximation is exploited to investigate the compressible flow through the receiver. Analytic solutions are obtained for the developments of air and ceramic temperatures as well as the pressure along the flow direction. Since the corresponding fluid and solid temperature variations generated under the Rosseland approximation agree fairly well with those based on the P1 model, the Rosseland approximation is used for further analysis. The results indicate that the pore diameter must be larger than its critical value to obtain high receiver efficiency. Moreover, it has been found that optimal pore diameter exists for achieving the maximum receiver efficiency under the equal pumping power. The solutions provide effective guidance for a novel volumetric solar receiver design of silicon carbide ceramic foam.

Keywords: turbulent heat transfer, thermal non-equilibrium, Rosseland approximation, P1 model, volumetric solar receiver, porous media, ceramic foam

1. Introduction

A solar volumetric receiver is required to have the resistance to temperature as high as 1000 degree Celsius, high porosity for sufficiently large extinction volume such that the concentrated solar radiation penetrates through the receiver, high cell density to achieve large specific surface area and sufficiently high effective thermal conductivity to avoid possible thermal spots. Extruded monoliths with parallel channels (i.e. honeycomb structure) are being used in some solar power plants in Europe, including the solar power tower plant of 1.5 MW built in 2009, in Julich in Germany [1, 2]. However, in such conventional receivers, both thermal spots [3] and flow instabilities [4] have been often reported. In the monolith receiver, locally high solar flux leads to a low mass flow with high temperature, whereas locally low solar flux leads to a high mass flow with low temperature. This causes the absorber material to exceed the design temperature locally, which then leads to its

destruction although the average temperature is comparatively low. These difficulties encountered in the receiver must be overcome to run the power plant safely.

In consideration of these requirements, ceramic foams have come to draw attention as a possible candidate to replace the conventional extruded monoliths with parallel channels. Many researchers including Becker et al. [4], Fend et al. [5] and Bai [6] focused on porous ceramic foams as a promising absorber material. Recently, Sano et al. [7] carried out a local non-thermal equilibrium analysis to investigate the receiver efficiency under the equal pumping power. For the first time, the complete set of analytical solutions based on the two-energy equation model of porous media was presented, so as to fully account for the combined effects of tortuosity; thermal dispersion and compressibility on the convective, conductive and radiative heat transfer within a ceramic foam receiver. In their analysis, however, the Rosseland approximation was applied to account for the radiative heat transfer through the solar receiver. It is well known that the Rosseland approximation ceases to be valid near boundaries. Although no wall boundaries exist for the case of the one-dimensional analysis of the solar volumetric receiver, the validity of applying the Rosseland approximation near the inlet boundary of the receiver has not been investigated yet. Furthermore, the effects of turbulence mixing on the heat transfer were not considered.

In this study, the validity of the Rosseland approximation [7] will be examined by comparing the results based on the Rosseland approximation and the results obtained from solving the irradiation transport equation based on the P1 model. The set of the equations will be reduced to a fifth-order ordinary differential equation for the air temperature. Once the air temperature distribution is determined, the pressure distribution along the flow direction can readily be estimated from the momentum equation with the low Mach approximation. Thus, the receiver efficiency, namely, the ratio of the air enthalpy flux increase to the concentrated solar heat flux, can be compared under the equal pumping power, so as to investigate the optimal operating conditions. Some analytical and numerical investigations [3–8] have been reported elsewhere. However, none of them appeared to elucidate well the combined effects of turbulence, compressibility, radiation, convection and conduction within the volumetric receiver on the developments of air and ceramic temperatures as well as the pressure along the flow direction. This study appears to be the first to provide the complete set of analytical solutions based on the two-energy equation model of porous media [9], fully accounting for the combined effects of turbulence, tortuosity, thermal dispersion, compressibility and radiative heat transfer within a ceramic foam receiver.

2. Volume averaged governing equations

As illustrated in **Figure 1**, the structure of silicon carbide ceramic foam volumetric receiver may be treated as homogeneous porous medium. Since the dependence of the Darcian velocity on the transverse direction can only be observed in a small region very close to the walls of the passage, we may neglect the boundary effects (i.e. Brinkman term).

Based on a theoretical derivation of Darcy's law, Neuman [10] pointed out that the application of Darcy's law to compressible fluids is justified as long as Knudsen numbers are sufficiently small to ensure the no-slip conditions at the solid–gas interface. This is usually the case for the volumetric receivers. Thus, allowing the density to vary through the receiver, the following Forchheimer extended Darcy law should hold:

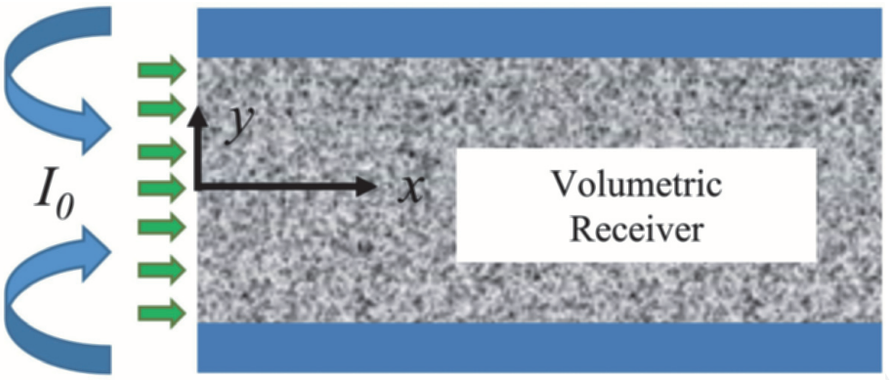

Figure 1.
Volumetric receiver.

$$-\frac{\partial\langle p\rangle^f}{\partial x_i}=\frac{\langle\mu\rangle^f}{K}\langle u_i\rangle+b\langle\rho\rangle^f\sqrt{\langle u_j\rangle\langle u_j\rangle}\langle u_i\rangle \tag{1}$$

where K and b are the permeability and the inertial coefficients, respectively. Furthermore, by virtue of the volume averaging procedure [11–13], the microscopic energy equations of the compressible fluid flow phase and the solid phase may be integrated over an elemental control volume V, so as to derive the corresponding macroscopic energy equations. Since the porous medium is considered to be homogeneous, the integration of the two distinct energy equations gives:

For the air:

$$\begin{aligned}&\varepsilon\frac{\partial}{\partial t}\left\langle\rho_f\left(h_{stag}-\frac{p}{\rho}\right)\right\rangle^f+\varepsilon\frac{\partial}{\partial x_j}\langle\rho\rangle^f\langle u_j\rangle^f\langle h_{st}\rangle^f\\&=\frac{\partial}{\partial x_j}\left(\varepsilon\langle k_f\rangle^f\frac{\partial\langle T\rangle^f}{\partial x_j}+\frac{1}{V}\int_{A_{\text{int}}}k_fTn_jdA-\varepsilon\langle\rho\rangle^f\left\langle\tilde{h}_{stag}\tilde{u}_j\right\rangle^f+\varepsilon\langle u_i\tau_{ij}\rangle^f\right)\\&\quad+\frac{1}{V}\int_{A_{\text{int}}}k_f\frac{\partial T}{\partial x_j}n_jdA\end{aligned} \tag{2}$$

For the solid matrix:

$$(1-\varepsilon)\rho_sc_s\frac{\partial\langle T\rangle^s}{\partial t}=\frac{\partial}{\partial x_j}\left((1-\varepsilon)k_s\frac{\partial\langle T\rangle^s}{\partial x_j}-\frac{k_s}{V}\int_{A_{\text{int}}}Tn_jdA\text{-}q_R\right)-\frac{1}{V}\int_{A_{\text{int}}}k_f\frac{\partial T}{\partial x_j}n_jdA \tag{3}$$

where the intrinsic volume average of a certain local variable ϕ in the fluid phase and solid matrix phase can be defined as.

$$\langle\phi\rangle^f\equiv\frac{1}{V_f}\int_{V_f}\phi dV,\langle\phi\rangle^m\equiv\frac{1}{V_m}\int_{V_m}\phi dV \tag{4}$$

Note that subscripts f and m refer to the fluid phase and solid matrix phase, respectively. The decomposition of the local variable ϕ can be expressed in terms of its intrinsic average and the spatial deviation from it:

$$\phi = \langle \phi \rangle^f + \tilde{\phi} \tag{5}$$

Moreover, q_R is the radiative heat flux, A_{int} is the interfacial surface area between the fluid and solid matrix phases, while n_j is the normal unit vector from the fluid phase to the solid matrix phase.

In order to simplify the foregoing set of the equations, the low Mach approximation is applied due to the relatively low Mach number when the air flows through a porous medium. Thus, the dynamic pressure change is sufficiently small as compared to the absolute pressure prevailing over the system, such that the stagnant enthalpy is approximated by $h_{stag} = h + u_k u_k/2 \cong h$. Combining the foregoing two energy equations namely Eqs. (2) and (3), and, then, noting the continuity of temperature and heat flux at the interface, we obtain the one-equation model for the steady state as follows:

$$\varepsilon \frac{\partial}{\partial x_j} \left\langle \rho_f \right\rangle^f \langle u_j \rangle^f \langle h \rangle^f = \frac{\partial}{\partial x_j} \left(\varepsilon \langle k_f \rangle^f \frac{\partial \langle T \rangle^f}{\partial x_j} + (1-\varepsilon) k_s \frac{\partial \langle T \rangle^s}{\partial x_j} + \frac{1}{V} \int_{A_{\text{int}}} (k_f - k_s) T n_j dA - \varepsilon \left\langle \rho_f \right\rangle^f \left\langle \tilde{h} \tilde{u}_j \right\rangle^f - q_R \right) \tag{6}$$

For the time being, let us assume $\partial \langle T \rangle^f / \partial x_j \cong \partial \langle T \rangle^s / \partial x_j \cong \partial \langle T \rangle / \partial x_j$ (this assumption will be relaxed shortly). Then, the equation reduces to

$$\varepsilon \frac{\partial}{\partial x_j} \left\langle \rho_f \right\rangle^f \langle u_j \rangle^f \langle h \rangle^f = \frac{\partial}{\partial x_j} \left(\left(\varepsilon \langle k_f \rangle^f + (1-\varepsilon) k_s \right) \frac{\partial \langle T \rangle}{\partial x_j} + \frac{1}{V} \int_{A_{\text{int}}} (k_f - k_s) T n_j dA - \varepsilon \left\langle \rho_f \right\rangle^f \left\langle \tilde{h} \tilde{u}_j \right\rangle^f - q_R \right) \tag{7}$$

where

$$\langle \phi \rangle \equiv \frac{1}{V} \int_V \phi dV \tag{8}$$

is the Darcian average of the variable ϕ such that $\langle u_j \rangle = \varepsilon \langle u_j \rangle^f$ is the Darcian velocity vector. From the foregoing equation, that is, Eq. (6), the macroscopic heat flux vector $q_i = \left(q_x, q_y, q_z \right)$ and its corresponding stagnant thermal conductivity k_{stag} may be defined as follows:

$$\begin{aligned} q_i &= -k_{stag} \frac{\partial \langle T \rangle}{\partial x_i} + q_R + \varepsilon \left\langle \rho_f \right\rangle^f \left\langle \tilde{h} \tilde{u}_i \right\rangle^f \\ &= -\left(\varepsilon \langle k_f \rangle^f + (1-\varepsilon) k_s \right) \frac{\partial \langle T \rangle}{\partial x_i} - \frac{1}{V} \int_{A_{\text{int}}} (k_f - k_s) T n_i dA + q_R + \varepsilon \left\langle \rho_f \right\rangle^f \left\langle \tilde{h} \tilde{u}_i \right\rangle^f \end{aligned} \tag{9}$$

or

$$k_{stag}\frac{\partial\langle T\rangle}{\partial x_i}=\left(\varepsilon\langle k_f\rangle^f+(1-\varepsilon)k_s\right)\frac{\partial\langle T\rangle}{\partial x_i}+\frac{1}{V}\int\limits_{A_{\text{int}}}\left(k_f-k_s\right)Tn_i dA \tag{10}$$

The term $\varepsilon\left\langle\rho_f\right\rangle^f\left\langle\tilde{h}\tilde{u}_i\right\rangle^f$ in Eq. (9) describes the thermal dispersion heat flux vector, which serves an additional heat flux resulting from the hydrodynamic mixing of fluid particles passing through pores. On the other hand, the second term on the right-hand side term in Eq. (10) is associated with the surface integral, and it describes the effects of the tortuosity on the macroscopic heat flux, which adjusts the level of the stagnant thermal conductivity from its upper bound $\left(\varepsilon k_f+(1-\varepsilon)k_s\right)$ to a correct one. Yang and Nakayama [9] introduced the effective porosity ε^*, which is defined as

$$\varepsilon^*=\frac{k_s-k_{stag}}{k_s-k_f}=\varepsilon+\frac{\varepsilon k_f+(1-\varepsilon)k_s-k_{stag}}{k_s-k_f} \tag{11}$$

such that

$$(\varepsilon^*-\varepsilon)\frac{\partial\langle T\rangle}{\partial x_i}=\frac{1}{V}\int_{A_{\text{int}}}Tn_i dA \tag{12}$$

Using the effective porosity ε^* and the equation of state $\langle p\rangle^f=\left\langle\rho_f\right\rangle^f R\langle T\rangle^f$ and $\langle h\rangle^f=c_p\langle T\rangle^f$, the volume average energy equations Eqs. (2) and (3) may be concisely rewritten for the steady state for air as:

$$\varepsilon c_p\frac{\partial}{\partial x_j}\left\langle\rho_f\right\rangle^f\langle u_j\rangle^f\langle T\rangle^f=\frac{\partial}{\partial x_j}\left(\varepsilon^*\langle k_f\rangle^f\frac{\partial\langle T\rangle^f}{\partial x_j}+\varepsilon k_{dis_{jk}}\frac{\partial\langle T\rangle^f}{\partial x_k}\right)-h_v\left(\langle T\rangle^f-\langle T\rangle^s\right) \tag{13}$$

for the solid matrix phase as:

$$\frac{\partial}{\partial x_j}\left((1-\varepsilon^*)k_s\frac{\partial\langle T\rangle^s}{\partial x_j}+q_R\right)-h_v\left(\langle T\rangle^s-\langle T\rangle^f\right)=0 \tag{14}$$

Note that the assumption of equal temperature gradients, $\partial\langle T\rangle^f/\partial x_j\cong\partial\langle T\rangle^s/\partial x_j\cong\partial\langle T\rangle/\partial x_j$, has been discarded. This practice has been proven to be quite effective in a series of computations (e.g. [8, 9]). According to the gradient diffusion hypothesis [14], the thermal dispersion term is usually expressed as:

$$\left\langle\rho_f\right\rangle^f\left\langle\tilde{h}\tilde{u}_j\right\rangle^f=\left\langle\rho_f\right\rangle^f c_p\left\langle\tilde{T}\tilde{u}_j\right\rangle^f=-k_{disjk}\frac{\partial\langle T\rangle^f}{\partial x_k} \tag{15}$$

while the interfacial heat transfer between the solid and fluid phases is modeled using Newton's cooling law:

$$\frac{1}{V}\int_{A_{\text{int}}}k_f\frac{\partial T}{\partial x_j}n_j dA=h_v\left(\langle T\rangle^s-\langle T\rangle^f\right) \tag{16}$$

where h_v is the volumetric heat transfer coefficient. The Maxwell approximations may be used for the dynamic viscosity and thermal conductivity of the air:

$$\mu\left(\langle T\rangle^f\right) = \mu_0\left(\frac{\langle T\rangle^f}{\langle T\rangle_0^f}\right)^n = 1.8\times10^{-5}\left(\frac{\langle T\rangle^f}{300K}\right)^{0.7}[\text{Pa}\cdot\text{s}] \tag{17}$$

and

$$k_f\left(\langle T\rangle^f\right) = k_0\left(\frac{\langle T\rangle^f}{\langle T\rangle_0^f}\right)^n = 0.025\left(\frac{\langle T\rangle^f}{300K}\right)^{0.7}[\text{W/mK}] \tag{18}$$

where the exponent n is 0.7 according to [4]. The specific heat capacity of the air $c_p = 1000[\text{J/kgK}]$ and the Prandtl number $Pr = 1.8\times10^{-5}\times1000/0.025 = 0.72$ are assumed to be constant.

3. One-dimensional analysis for volumetric receiver

In this section, we perform one-dimensional analysis to obtain analytic solutions for convective-radiative heat transfer in volume receiver. Prior to that, the radiative heat flux q_R needs to be determined in advance. In the literature, there are two models, namely, the Rosseland approximation and the P1 model.

3.1 Analysis based on the Rosseland approximation

In the Rosseland approximation, the radiative heat flux is given by

$$q_R = -\frac{16\sigma}{3\beta}(\langle T\rangle^s)^3\frac{\partial\langle T\rangle^s}{\partial x_j} \tag{19}$$

where $\sigma = 5.67\times10^{-8}\left[\text{W/m}^2\text{K}^4\right]$ is the Stephan-Boltzmann constant while β is the mean extinction coefficient.

As schematically shown in **Figure 1**, the air is flowing through a passage of length L at the rate of the mass flux $G = \left\langle\rho_f\right\rangle^f\langle u\rangle$. Under the low Mach number approximation, namely, $\left\langle\rho_f\right\rangle^f \propto 1/\langle T\rangle^f$, the macroscopic governing equations Eqs. (1), (13) and (14) can be simplified to be a one-dimensional set of equations as follows:

$$-\frac{d\langle p\rangle^f}{dx} = \frac{\langle\mu\rangle^f}{K}\frac{G}{\left\langle\rho_f\right\rangle^f} + b\frac{G^2}{\left\langle\rho_f\right\rangle^f} = \frac{R}{\langle p\rangle^f}\left(\frac{\langle\mu\rangle^f}{K}G + bG^2\right)\langle T\rangle^f \tag{20}$$

$$c_pG\frac{d\langle T\rangle^f}{dx} = \frac{d}{dx}\left(\varepsilon^*\left\langle k_f\right\rangle^f + \varepsilon k_{disxx}\right)\frac{d\langle T\rangle^f}{dx} - h_v\left(\langle T\rangle^f - \langle T\rangle^s\right) \tag{21}$$

$$\frac{d}{dx}\left((1-\varepsilon^*)k_s + \frac{16\sigma}{3\beta}(\langle T\rangle^s)^3\right)\frac{d\langle T\rangle^s}{dx} - h_v\left(\langle T\rangle^s - \langle T\rangle^f\right) = 0 \tag{22}$$

According to Calmidi and Mahajan [15, 16], Dukhan [17], Kuwahara et al. [18] and Yang et al. [19, 20], the permeability and inertial coefficient of foams are given by

$$K = 0.00073(1-\varepsilon)^{-0.224}\left(\frac{1.18}{1-e^{-(1-\varepsilon)/0.04}}\sqrt{\frac{1-\varepsilon}{3\pi}}\right)^{-1.11} {d_m}^2 \tag{23}$$

and

$$b = \frac{12(1-\varepsilon)}{d_m} \tag{24}$$

respectively, where d_m is the pore diameter of foam. The longitudinal dispersion coefficient is roughly about 20 times more than the transverse one. Thus, following Calmidi and Mahajan [16], we may evaluate the longitudinal dispersion coefficient using the following expression:

$$\varepsilon k_{dis_{xx}} = 1.2 c_p G\sqrt{K} \tag{25}$$

With respect to the stagnant thermal conductivity and the volumetric heat transfer coefficient for foams, Calmidi and Mahajan [15, 16] empirically provided the following correlations:

$$k_{stag} = \varepsilon k_f + 0.19(1-\varepsilon)^{0.763} k_s \tag{26}$$

$$h_v = 8.72(1-\varepsilon)^{1/4}\left(\frac{1-e^{-(1-\varepsilon)/0.04}}{\varepsilon}\right)^{1/2}\left(\frac{G d_m}{\langle\mu\rangle^f}\right)^{1/2} Pr^{0.37}\frac{k_f}{{d_m}^2} \tag{27}$$

Kamiuto et al. [21] experimentally affirmed that the Rosseland model is quite effective. Therefore, it can be deduced that the Rosseland model is also applicable for the present case of silicon carbide ceramic foam. Based on the measurements made on cordierite ceramic foams by Kamiuto et al., the mean extinction coefficient β is calculated by the following correlation:

$$\beta = 8(1-\varepsilon)/d_m \tag{28}$$

For a given mass flux $G = \left\langle \rho_f \right\rangle^f \langle u \rangle$, the foregoing three equations along with the equation of state may be solved for the four unknowns, namely, $\langle T\rangle^f$,$\langle T\rangle^s$, $\langle p\rangle^f$ and $\left\langle \rho_f \right\rangle^f$. The boundary conditions are given as follows:

$x = 0$ (inlet):

$$\langle T\rangle^f = \langle T\rangle_0^f = 300[\mathrm{K}] \tag{29}$$

$$\langle p\rangle^f = \langle p\rangle_0^f = 10^5[\mathrm{P}a] \tag{30}$$

such that $\left\langle \rho_f \right\rangle^f = \left\langle \rho_f \right\rangle_0^f = \langle p\rangle_0^f / R\langle T\rangle_0^f = 10^5/(287\times 300) = 1.2[\mathrm{kg/m^3}]$

$$-\left(\varepsilon^*\left\langle k_f\right\rangle^f + \varepsilon k_{disxx}\right)\frac{d\langle T\rangle^f}{dx}\bigg|_{x=0} - \left((1-\varepsilon^*)k_s + \frac{16\sigma}{3\beta}(\langle T\rangle^s)^3\right)\frac{d\langle T\rangle^s}{dx}\bigg|_{x=0}$$
$$= I_0\cos\xi - (1-\varepsilon)\left(a\sigma\left(\left(\langle T\rangle_0^s\right)^4 - \left(\langle T\rangle_0^f\right)^4\right) + h_{conv}\left(\langle T\rangle_0^s - \langle T\rangle_0^f\right)\right) \tag{31}$$

where I_0 is the intensity of radiation and ξ is the incidence angle. Moreover, $a \cong 0.9$ is the emissivity of the front surface of the receiver, while h_{conv} is the convective heat transfer coefficient at the frontal surface. The properties of the air depend on the temperature, which makes the integrations of the foregoing governing equations formidable. In order to obtain analytic expressions for the unknown variables, we may approximate these properties by their representative values evaluated at the average air temperature over the receiver as given by

$$\overline{\langle T\rangle^f} = \frac{1}{L}\int_0^L \langle T\rangle^f dx \tag{32}$$

Likewise we shall define the solid phase average temperature as follows:

$$\overline{\langle T\rangle^s} = \frac{1}{L}\int_0^L \langle T\rangle^s dx \tag{33}$$

The two energy equations, that is, Eqs. (21) and (22) may be added together and integrated using the boundary conditions in Eqs. (29) and (31) to give

$$\begin{aligned} c_p G\left(\langle T\rangle^f - \langle T\rangle_0^f\right) = {} & \left(\varepsilon^* k_0 \left(\frac{\overline{\langle T\rangle^f}}{\langle T\rangle_0^f}\right)^n + \varepsilon k_{disxx}\right)\frac{d\langle T\rangle^f}{dx} \\ & + \left((1-\varepsilon^*)k_s + \frac{16\sigma}{3\beta}\left(\overline{\langle T\rangle^s}\right)^3\right)\frac{d\langle T\rangle^s}{dx} + I_0\cos\xi \\ & - (1-\varepsilon)\left(a\sigma\left(\left(\langle T\rangle_0^s\right)^4 - \left(\langle T\rangle_0^f\right)^4\right) + h_{\cov}\left(\langle T\rangle_0^s - \langle T\rangle_0^f\right)\right) \end{aligned} \tag{34}$$

This equation is substituted into Eq. (21) to eliminate $\langle T\rangle^s$ in favor of $\langle T\rangle^f$. The resulting ordinary differential equation for $\langle T\rangle^f$ runs as

$$\begin{aligned} \frac{d^3\langle T\rangle^f}{dx^3} = {} & \frac{Gc_p}{\varepsilon^* k_0\left(\frac{\overline{\langle T\rangle^f}}{\langle T\rangle_0^f}\right)^n + \varepsilon k_{disxx}}\frac{d^2\langle T\rangle^f}{dx^2} \\ & + h_v \frac{k_{stag} + \varepsilon k_{disxx} + \frac{16\sigma}{3\beta}\left(\overline{\langle T\rangle^s}\right)^3}{\left(\varepsilon^* k_0\left(\frac{\overline{\langle T\rangle^f}}{\langle T\rangle_0^f}\right)^n + \varepsilon k_{disxx}\right)\left((1-\varepsilon^*)k_s + \frac{16\sigma}{3\beta}\left(\overline{\langle T\rangle^s}\right)^3\right)}\frac{d\langle T\rangle^f}{dx} \\ & - h_v \frac{Gc_p}{\left(\varepsilon^* k_0\left(\frac{\overline{\langle T\rangle^f}}{\langle T\rangle_0^f}\right)^n + \varepsilon k_{disxx}\right)\left((1-\varepsilon^*)k_s + \frac{16\sigma}{3\beta}\left(\overline{\langle T\rangle^s}\right)^3\right)}\langle T\rangle^f \\ & + h_v \frac{I_0\cos\xi - (1-\varepsilon)\left(a\sigma\left(\left(\langle T\rangle_0^s\right)^4 - \left(\langle T\rangle_0^f\right)^4\right) + h_{\cov}\left(\langle T\rangle_0^s - \langle T\rangle_0^f\right)\right)}{\left(\varepsilon^* k_0\left(\frac{\overline{\langle T\rangle^f}}{\langle T\rangle_0^f}\right)^n + \varepsilon k_{disxx}\right)\left((1-\varepsilon^*)k_s + \frac{16\sigma}{3\beta}\left(\overline{\langle T\rangle^s}\right)^3\right)} \end{aligned} \tag{35}$$

This ordinary differential equation, with the boundary conditions in Eqs. (29), (30) and (31) and the auxiliary asymptotic condition $d\langle T\rangle_0^f/dx = d^2\langle T\rangle_0^f/dx^2 = 0$, yields

$$\langle T\rangle^f = T_{eq} - \left(T_{eq} - \langle T\rangle_0^f\right)e^{-\gamma\lambda x} \tag{36}$$

and

$$\langle T\rangle^s = T_{eq} - \left(T_{eq} - \langle T\rangle_0^s\right)e^{-\gamma\lambda x} \tag{37}$$

where γ is the positive real root, which can uniquely be determined from the following cubic equation:

$$\gamma^3 + \frac{Gc_p}{\left(\varepsilon^* k_0\left(\frac{\overline{\langle T\rangle^f}}{\langle T\rangle_0^f}\right)^n + \varepsilon k_{disxx}\right)\lambda}\gamma^2 - \gamma - \frac{Gc_p}{\left(k_{stag} + \varepsilon k_{disxx} + \frac{16\sigma}{3\beta}\left(\overline{\langle T\rangle^s}\right)^3\right)\lambda} = 0 \tag{38}$$

where

$$\lambda = \sqrt{\frac{\left(k_{stag} + \varepsilon k_{disxx} + \frac{16\sigma}{3\beta}\left(\overline{\langle T\rangle^s}\right)^3\right)h_v}{\left(\varepsilon^* k_0\left(\frac{\overline{\langle T\rangle^f}}{\langle T\rangle_0^f}\right)^n + \varepsilon k_{disxx}\right)\left((1-\varepsilon^*)k_s + \frac{16\sigma}{3\beta}\left(\overline{\langle T\rangle^s}\right)^3\right)}} \tag{39}$$

The solid phase temperature at the inlet $\langle T\rangle_0^s$ and temperature at the thermal equilibrium, namely, $T_{eq} = \langle T\rangle_\infty^f = \langle T\rangle_\infty^s$, are given by

$$\langle T\rangle_0^s = T_{eq} + \left(T_{eq} - \langle T\rangle_0^f\right)\frac{Gc_p + \left(\varepsilon^* k_0\left(\frac{\overline{\langle T\rangle^f}}{\langle T\rangle_0^f}\right)^n + \varepsilon k_{disxx}\right)\gamma\lambda}{\left((1-\varepsilon^*)k_s + \frac{16\sigma}{3\beta}\left(\overline{\langle T\rangle^s}\right)^3\right)\gamma\lambda} \tag{40}$$

and

$$T_{eq} = \langle T\rangle_0^f + \frac{I_0\cos\xi - (1-\varepsilon)\left(a\sigma\left(\left(\langle T\rangle_0^s\right)^4 - \left(\langle T\rangle_0^f\right)^4\right) + h_{\text{cov}}\left(\langle T\rangle_0^s - \langle T\rangle_0^f\right)\right)}{Gc_p} \tag{41}$$

respectively. Usually, the receiver length L is sufficiently long to reach the local thermal equilibrium. Thus, the average air and solid temperatures are evaluated from

$$\overline{\langle T\rangle^f} = \frac{1-e^{-\gamma\lambda L}}{\gamma\lambda L}\langle T\rangle_0^f + \left(1 - \frac{1-e^{-\gamma\lambda L}}{\gamma\lambda L}\right)T_{eq} \cong \frac{1}{\gamma\lambda L}\langle T\rangle_0^f + \left(1 - \frac{1}{\gamma\lambda L}\right)T_{eq} \tag{42}$$

$$\overline{\langle T\rangle^s} = \frac{1-e^{-\gamma\lambda L}}{\gamma\lambda L}\langle T\rangle_0^s + \left(1 - \frac{1-e^{-\gamma\lambda L}}{\gamma\lambda L}\right)T_{eq} \cong \frac{1}{\gamma\lambda L}\langle T\rangle_0^s + \left(1 - \frac{1}{\gamma\lambda L}\right)T_{eq} \tag{43}$$

As one of the most important performance parameters, the receiver efficiency is defined by

$$\eta = \frac{I_0 \cos\xi - (1-\varepsilon)\left(a\sigma\left(\left(\langle T\rangle_0^s\right)^4 - \left(\langle T\rangle_0^f\right)^4\right) + h_{\text{cov}}\left(\langle T\rangle_0^s - \langle T\rangle_0^f\right)\right)}{I_0 \cos\xi} \tag{44}$$

Having established the temperature development, the momentum equation, that is, Eq. (20) along with the equation of state can easily be solved to find out the pressure distribution along the receiver as

$$\langle p\rangle^f = \sqrt{\left(\langle p\rangle_0^f\right)^2 - 2R\left(\frac{\mu_0}{K}\left(\frac{\overline{\langle T\rangle^f}}{\langle T\rangle_0^f}\right)^n G + bG^2\right)\left(\frac{1-e^{-\gamma\lambda x}}{\gamma\lambda}\langle T\rangle_0^f + \left(x - \frac{1-e^{-\gamma\lambda x}}{\gamma\lambda}\right)T_{eq}\right)} \tag{45}$$

Under the low Mach approximation, the required pumping power per unit frontal area may be evaluated from

$$PP = G\int_0^L -\frac{d\langle p\rangle^f}{\left\langle\rho_f\right\rangle^f} = G\int_0^L -\frac{1}{\left\langle\rho_f\right\rangle^f}\frac{d\langle p\rangle^f}{dx}dx$$

$$= \left(\frac{R}{\langle p\rangle_0^f}\right)^2 G\left(\frac{\mu_0}{K}\left(\frac{\overline{\langle T\rangle^f}}{\langle T\rangle_0^f}\right)^n G + bG^2\right)\int_0^L \left(\langle T\rangle^f\right)^2 dx$$

$$= \left(\frac{R}{\langle p\rangle_0^f}\right)^2 G\left(\frac{\mu_0}{K}\left(\frac{\overline{\langle T\rangle^f}}{\langle T\rangle_0^f}\right)^n G + bG^2\right)L\left({T_{eq}}^2 - \frac{2\left(1-e^{-\gamma\lambda L}\right)}{\gamma\lambda L}T_{eq}\left(T_{eq} - \langle T\rangle_0^f\right)\right.$$

$$\left. + \frac{1-e^{-2\gamma\lambda L}}{2\gamma\lambda L}\left(T_{eq} - \langle T\rangle_0^f\right)^2\right)$$

$$\cong \frac{G}{\left(\langle\rho\rangle_0^f\right)^2}\left(\frac{\mu_0}{K}\left(\frac{\overline{\langle T\rangle^f}}{\langle T\rangle_0^f}\right)^n G + bG^2\right)\frac{1}{2\gamma\lambda}\left((2\gamma\lambda L - 3)\left(\frac{T_{eq}}{\langle T\rangle_0^f}\right)^2 + 2\left(\frac{T_{eq}}{\langle T\rangle_0^f}\right) + 1\right) \tag{46}$$

Note that the dynamic pressure change is sufficiently small as compared to the absolute pressure such that $\left\langle\rho_f\right\rangle^f \propto 1/\langle T\rangle^f$.

3.2 Analysis based on the P1 model

Since the Rosseland approximation used in the previous analysis ceases to be valid near boundaries, the validity of applying the Rosseland approximation near the inlet boundary of the receiver should be investigated. In order to examine the validity of the Rosseland approximation, the results based on the Rosseland approximation will be compared with the results obtained from solving the irradiation transport equation based on the P1 model. Since the silicon carbide ceramic

foam is optically thick, the radiant energy emitted from other locations in the domain is quickly absorbed such that the radiative heat flux is given by

$$q_R = -\frac{1}{3\beta}\frac{\partial G}{\partial x_j} \tag{47}$$

where the diffuse integrated intensity G_r satisfies the irradiation transport equation based on the P1 model as follows:

$$\frac{\partial}{\partial x_j}\left(\frac{1}{3\beta}\frac{\partial G_r}{\partial x_j}\right) + \kappa\left(4\sigma(\langle T\rangle^s)^4 - G_r\right) = 0 \tag{48}$$

where κ is the absorption coefficient.

Moreover, the effects of turbulence mixing on the heat transfer are also considered. Therefore, the energy equation for the air will be written as

$$\varepsilon c_p \frac{\partial}{\partial x_j}\left\langle \rho_f \right\rangle^f \langle u_j\rangle^f \langle T\rangle^f = \frac{\partial}{\partial x_j}\left(\varepsilon^* \left\langle k_f \right\rangle^f \frac{\partial \langle T\rangle^f}{\partial x_j} + \varepsilon\left(k_{dis_{jk}} + \frac{c_{p_f}\langle \mu_t\rangle^f}{\sigma_T}\right)\frac{\partial \langle T\rangle^f}{\partial x_k}\delta_{jk}\right) - h_v\left(\langle T\rangle^f - \langle T\rangle^s\right) \tag{49}$$

where turbulent Prandtl number $\sigma_T = 0.9$ is assumed to be constant.

Under the low Mach number approximation, namely, we may reduce the macroscopic governing equations namely Eqs. (1), (49), (14) and (48) to a one-dimensional set of the equations as follows:

$$-\frac{d\langle p\rangle^f}{dx} = \frac{\langle \mu\rangle^f}{K}\frac{G}{\left\langle \rho_f \right\rangle^f} + b\frac{G^2}{\left\langle \rho_f \right\rangle^f} = \frac{R}{\langle p\rangle^f}\left(\frac{\langle \mu\rangle^f}{K}G + bG^2\right)\langle T\rangle^f \tag{50}$$

$$c_p G\frac{d\langle T\rangle^f}{dx} = \frac{d}{dx}\left(\varepsilon^* \left\langle k_f \right\rangle^f + \varepsilon\left(k_{dis_{xx}} + \frac{c_{p_f}\langle \mu_t\rangle^f}{\sigma_T}\right)\right)\frac{d\langle T\rangle^f}{dx} - h_v\left(\langle T\rangle^f - \langle T\rangle^s\right) \tag{51}$$

$$\frac{d}{dx}\left((1-\varepsilon^*)k_s\frac{d\langle T\rangle^s}{dx} + \frac{1}{3\beta}\frac{dG_r}{dx}\right) - h_v\left(\langle T\rangle^s - \langle T\rangle^f\right) = 0 \tag{52}$$

$$\frac{d}{dx}\left(\frac{1}{3\beta}\frac{dG_r}{dx}\right) + \kappa\left(4\sigma(\langle T\rangle^s)^4 - G_r\right) = 0 \tag{53}$$

The turbulence kinetic energy is dropped from the momentum equation since it stays nearly constant within the receiver.

Nakayama and Kuwahara [22] established the macroscopic two-equation turbulence model, which does not require any detailed morphological information for the structure. The model, for given permeability and Forchheimer coefficient, can be used for analyzing most complex turbulent flow situations in homogeneous porous media. For the case of fully developed turbulent flow in an isotropic porous structure, the eddy viscosity is given by

$$\langle \mu_t \rangle^f = 2GbK \tag{54}$$

Note that

$$k_{dis_{xx}} / \left(c_{p_f} \langle \mu_t \rangle^f / \sigma_T \right) = 0.6\sigma_T / \varepsilon b \sqrt{K} > 1$$

such that the dispersion thermal conductivity usually overwhelms the eddy thermal conductivity.

For absorption coefficient κ, the measurements made on cordierite ceramic foams by Kamiuto et al. [22] give the following correlation:

$$\kappa = 4a(1-\varepsilon)/d_m \tag{55}$$

The boundary conditions of $\langle T \rangle^f$ and $\langle p \rangle^f$ are the same as Eqs. (29) and (30). The other boundary conditions are given as follows:

$$q_{R_x} = -\frac{1}{3\beta}\frac{dG_r}{dx} = -\frac{G_r}{2} \tag{56}$$

and

$$\begin{aligned} &-\left(\varepsilon^* \langle k_f \rangle^f + \varepsilon \left(k_{disxx} + \frac{c_{p_f} \langle \mu_t \rangle^f}{\sigma_T} \right) \right) \frac{d\langle T \rangle^f}{dx}\bigg|_{x=0} - (1-\varepsilon^*) k_s \frac{d\langle T \rangle^s}{dx}\bigg|_{x=0} - \frac{G_r|_{x=0}}{2} \\ &= (1-(1-a)(1-\varepsilon)) I_0 \cos\xi \\ &\quad - (1-\varepsilon)\left(a\sigma\left(\left(\langle T \rangle_0^s \right)^4 - \left(\langle T \rangle_0^f \right)^4 \right) + h_{conv}\left(\langle T \rangle_0^s - \langle T \rangle_0^f \right) \right) \end{aligned} \tag{57}$$

Furthermore, the streamwise gradients of the dependent variables $\langle T \rangle^f$, $\langle T \rangle^s$ and G_r are set to zero sufficiently far downstream at $x = L$.

The two energy equations, namely, Eqs. (51) and (52) may be added together and integrated using the boundary conditions in Eqs. (29) and (57) to give

$$\begin{aligned} &c_p G\left(\langle T \rangle^f - \langle T \rangle_0^f \right) \\ &= \left(\varepsilon^* k_0 \left(\frac{\overline{\langle T \rangle^f}}{\langle T \rangle_0^f} \right)^n + \varepsilon \left(k_{dis_{xx}} + \frac{c_{p_f} \langle \mu_t \rangle^f}{\sigma_T} \right) \right) \frac{d\langle T \rangle^f}{dx} + (1-\varepsilon^*) k_s \frac{\partial \langle T \rangle^s}{\partial x_j} + \frac{1}{3\beta}\frac{dG_r}{dx} \\ &+ (1-(1-a)(1-\varepsilon)) I_0 \cos\xi - (1-\varepsilon)\left(a\sigma\left(\left(\langle T \rangle_0^s \right)^4 - \left(\langle T \rangle_0^f \right)^4 \right) + h_{conv}\left(\langle T \rangle_0^s - \langle T \rangle_0^f \right) \right) \end{aligned} \tag{58}$$

Eqs. (52) and (53) are combined to give

$$G_r = 4\sigma(\langle T \rangle^s)^4 + \frac{h_v}{\kappa}\left(\langle T \rangle^s - \langle T \rangle^f \right) - \frac{(1-\varepsilon^*) k_s}{\kappa}\frac{d^2\langle T \rangle^s}{dx^2} \tag{59}$$

This equation, Eq. (59), and Eq. (51) are substituted into Eq. (58) to eliminate G_r and $\langle T \rangle^s$ in favor of $\langle T \rangle^f$. The resulting ordinary differential equation for $\langle T \rangle^f$ runs as

$$\frac{d^5\langle T\rangle^f}{dx^5} = \frac{Gc_p}{\varepsilon^* k_0\left(\frac{\overline{\langle T\rangle^f}}{\langle T\rangle_0^f}\right)^n + \varepsilon\left(k_{dis_{xx}} + \frac{c_{p_f}\langle \mu_t\rangle^f}{\sigma_T}\right)}\frac{d^4\langle T\rangle^f}{dx^4}$$
$$+\left(3\beta\kappa\frac{(1-\varepsilon^*)k_s + \frac{16\sigma}{3\beta}\left(\overline{\langle T\rangle^s}\right)^3 + \frac{h_v}{3\beta\kappa}}{(1-\varepsilon^*)k_s} + \frac{h_v}{\varepsilon^* k_0\left(\frac{\overline{\langle T\rangle^f}}{\langle T\rangle_0^f}\right)^n + \varepsilon\left(k_{dis_{xx}} + \frac{c_{p_f}\langle \mu_t\rangle^f}{\sigma_T}\right)}\right)\frac{d^3\langle T\rangle^f}{dx^3}$$
$$-\left((1-\varepsilon^*)k_s + \frac{16\sigma}{3\beta}\left(\overline{\langle T\rangle^s}\right)^3 + \frac{h_v}{3\beta\kappa}\right)\frac{3\beta\kappa Gc_p}{\left(\varepsilon^* k_0\left(\frac{\overline{\langle T\rangle^f}}{\langle T\rangle_0^f}\right)^n + \varepsilon\left(k_{dis_{xx}} + \frac{c_{p_f}\langle \mu_t\rangle^f}{\sigma_T}\right)\right)(1-\varepsilon^*)k_s}\frac{d^2\langle T\rangle^f}{dx^2}$$
$$-3\beta\kappa h_v\frac{k_{stag} + \varepsilon\left(k_{dis_{jk}} + \frac{c_{p_f}\langle \mu_t\rangle^f}{\sigma_T}\right) + \frac{16\sigma}{3\beta}\left(\overline{\langle T\rangle^s}\right)^3}{\left(\varepsilon^* k_0\left(\frac{\overline{\langle T\rangle^f}}{\langle T\rangle_0^f}\right)^n + \varepsilon\left(k_{dis_{xx}} + \frac{c_{p_f}\langle \mu_t\rangle^f}{\sigma_T}\right)\right)(1-\varepsilon^*)k_s}\frac{d\langle T\rangle^f}{dx}$$
$$+\frac{3\beta\kappa h_v Gc_p}{\left(\varepsilon^* k_0\left(\frac{\overline{\langle T\rangle^f}}{\langle T\rangle_0^f}\right)^n + \varepsilon\left(k_{dis_{xx}} + \frac{c_{p_f}\langle \mu_t\rangle^f}{\sigma_T}\right)\right)(1-\varepsilon^*)k_s}\left(\langle T\rangle^f - \langle T\rangle_0^f\right)$$
$$-3\beta\kappa h_v\frac{(1-(1-a)(1-\varepsilon))I_0\cos\xi - (1-\varepsilon)\left(a\sigma\left(\left(\langle T\rangle_0^s\right)^4 - \left(\langle T\rangle_0^f\right)^4\right) + h_{conv}\left(\langle T\rangle_0^s - \langle T\rangle_0^f\right)\right)}{\left(\varepsilon^* k_0\left(\frac{\overline{\langle T\rangle^f}}{\langle T\rangle_0^f}\right)^n + \varepsilon\left(k_{dis_{xx}} + \frac{c_{p_f}\langle \mu_t\rangle^f}{\sigma_T}\right)\right)(1-\varepsilon^*)k_s} \tag{60}$$

This ordinary differential equation, with the boundary conditions in Eqs. (29), (56) and (57) and the zero derivative conditions far downstream ($x \to \infty$: Note L is sufficiently large), yields Eqs. (36) and (37). Note that γ is the positive real root which can be determined from the following characteristic equation:

$$\gamma^5 + \frac{Gc_p}{\left(\varepsilon^* k_0\left(\frac{\overline{\langle T\rangle^f}}{\langle T\rangle_0^f}\right)^n + \varepsilon\left(k_{dis_{xx}} + \frac{c_{p_f}\langle \mu_t\rangle^f}{\sigma_T}\right)\right)\lambda}\gamma^4$$
$$-\frac{\frac{3\beta\kappa}{h_v}\left(\varepsilon^* k_0\left(\frac{\overline{\langle T\rangle^f}}{\langle T\rangle_0^f}\right)^n + \varepsilon\left(k_{dis_{xx}} + \frac{c_{p_f}\langle \mu_t\rangle^f}{\sigma_T}\right)\right)\left((1-\varepsilon^*)k_s + \frac{16\sigma}{3\beta}\left(\overline{\langle T\rangle^s}\right)^3 + \frac{h_v}{3\beta\kappa}\right) + (1-\varepsilon^*)k_s}{k_{stag} + \varepsilon\left(k_{dis_{xx}} + \frac{c_{p_f}\langle \mu_t\rangle^f}{\sigma_T}\right) + \frac{16\sigma}{3\beta}\left(\overline{\langle T\rangle^s}\right)^3}\gamma^3$$
$$-\frac{(1-\varepsilon^*)k_s + \frac{16\sigma}{3\beta}\left(\overline{\langle T\rangle^s}\right)^3 + \frac{h_v}{3\beta\kappa}}{k_{stag} + \varepsilon\left(k_{dis_{xx}} + \frac{c_{p_f}\langle \mu_t\rangle^f}{\sigma_T}\right) + \frac{16\sigma}{3\beta}\left(\overline{\langle T\rangle^s}\right)^3}\frac{3\beta\kappa Gc_p}{h_v\lambda}\gamma^2 + \frac{3\beta\kappa}{\lambda^2}\gamma$$
$$+\frac{3\beta\kappa Gc_p}{\left(k_{stag} + \varepsilon\left(k_{dis_{xx}} + \frac{c_{p_f}\langle \mu_t\rangle^f}{\sigma_T}\right) + \frac{16\sigma}{3\beta}\left(\overline{\langle T\rangle^s}\right)^3\right)\lambda^3} = 0 \tag{61}$$

where

$$\lambda = \sqrt{\frac{\left(k_{stag} + \varepsilon\left(k_{dis_{xx}} + \frac{c_{p_f}\langle\mu_t\rangle^f}{\sigma_T}\right) + \frac{16\sigma}{3\beta}\left(\overline{\langle T\rangle^s}\right)^3\right)h_v}{\left(\varepsilon^* k_0\left(\frac{\overline{\langle T\rangle^f}}{\langle T\rangle_0^f}\right)^n + \varepsilon\left(k_{dis_{xx}} + \frac{c_{p_f}\langle\mu_t\rangle^f}{\sigma_T}\right)\right)(1-\varepsilon^*)k_s}} \tag{62}$$

The solid phase temperature at the inlet $\langle T\rangle_0^s$ and temperature at the thermal equilibrium, namely, $T_{eq} = \langle T\rangle_\infty^f = \langle T\rangle_\infty^s$, are determined from the following implicit equations:

$$\begin{aligned} Gc_p\left(T_{eq} - \langle T\rangle_0^f\right) = &-\left(\varepsilon^* k_0 + \varepsilon\left(k_{dis_{xx}} + \frac{c_{p_f}\langle\mu_t\rangle^f}{\sigma_T}\right)\right)\gamma\lambda\left(T_{eq} - \langle T\rangle_0^f\right) \\ &- (1-\varepsilon^*)k_s\gamma\lambda\left(T_{eq} - \langle T\rangle_0^s\right) \\ &- \frac{1}{2}\left(4\sigma\left(\langle T\rangle_0^s\right)^4 + \frac{h_v}{\kappa}\left(\langle T\rangle_0^s - \langle T\rangle_0^f\right) + \frac{(1-\varepsilon^*)k_s}{\kappa}(\gamma\lambda)^2\left(T_{eq} - \langle T\rangle_0^s\right)\right) \end{aligned} \tag{63}$$

$$\begin{aligned} T_{eq} = &\langle T\rangle_0^f \\ &+ \frac{(1-(1-a)(1-\varepsilon))I_0\cos\xi - (1-\varepsilon)\left(a\sigma\left(\left(\langle T\rangle_0^s\right)^4 - \left(\langle T\rangle_0^f\right)^4\right) + h_{conv}\left(\langle T\rangle_0^s - \langle T\rangle_0^f\right)\right)}{Gc_p} \end{aligned} \tag{64}$$

where the boundary condition in Eq. (56) is utilized. Usually, the receiver length L is sufficiently long to reach the local thermal equilibrium. Thus, the average air and solid temperatures are evaluated from Eqs. (42) and (43).

4. Validations of the Rosseland approximation

Smirnova et al. [23] numerically studied the compressible fluid flow and heat transfer within the solar receiver with silicon carbide monolithic honeycombs. In their paper, the following input data were collected to obtain the analytic solutions based on the present local thermal non-equilibrium model:

$$\left\langle \rho_f \right\rangle_0^f = 1.2[\mathrm{kg/m^3}],\ \langle T\rangle_0^f = 300[\mathrm{K}](\langle p\rangle_0^f = 10^5[\mathrm{Pa}]),\ c_p = 1000[\mathrm{J/kgK}],$$
$$G = 1.2[\mathrm{kg/m^2s}],\ L = 0.05[m],\ I_0 = 10^6[\mathrm{W/m^2}],\ \xi = 0,\ h_{conv} = 0[\mathrm{W/m^2K}],$$
$$k_s = 150[\mathrm{W/mK}]k_{dis} = 0[\mathrm{W/mK}],\ h_v = 8.8\times10^4[\mathrm{W/m^3K}],\ \varepsilon = 0.5,\ \beta = 50[1/\mathrm{m}].$$

However, it should be noticed that the porosity of the silicon carbide monolithic honeycombs is not available in Smirnova et al. [23], its value was estimated to be $\varepsilon = 0.5$ from the figure provided by Agrafiotis et al. [24]. The mean extinction coefficient β for silicon carbide monolithic honeycombs is not available in their paper. Finally, the value was estimated to be 50[1/m] by correlating the present results against theirs. It should also be noted that the convective heat transfer coefficient was set to zero since radiation predominates over convection in the receiver front.

As for possible instabilities, the fifth-order characteristic Eq. (61) based on the P1 model should be examined carefully. **Figure 2** shows the residual of the fifth-order characteristic equation $f_R(\gamma)$. The figure clearly shows that the fifth-order

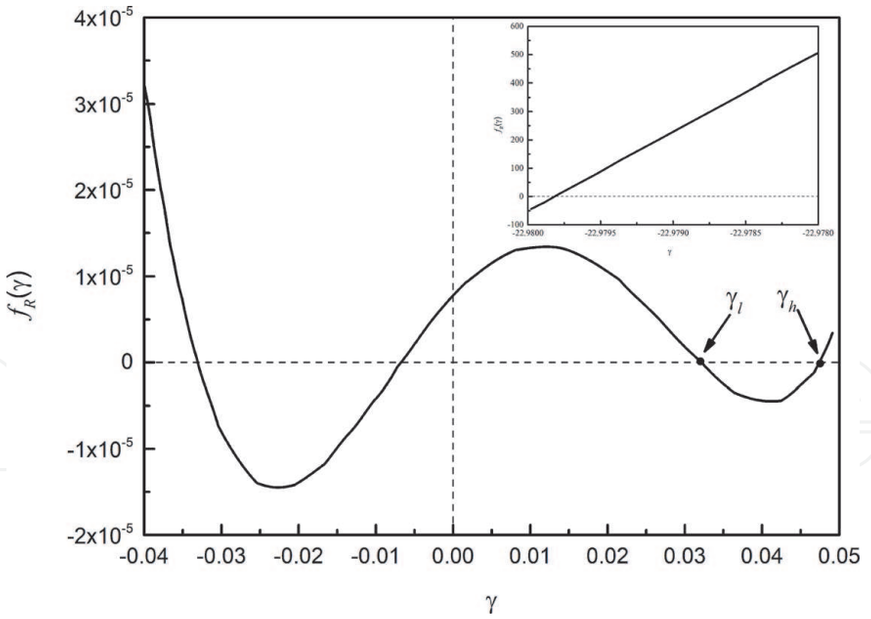

Figure 2.
Residual of the fifth-order characteristic equation.

characteristic Eq. (61) under a possible range of the silicon carbide parameters yields two positive roots γ_h and γ_l, which are fairly close to each other. The corresponding temperature variations of both phases however depend strongly on its value, which results in a non-unique value of equilibrium temperature. Since flow instability is inferred by an unexpected nature of the quadratic pressure difference with respect to equilibrium temperature, the existence of two positive roots may be responsible for possible hydrodynamic and thermal instabilities reported previously. A further investigation based on an unsteady procedure is definitely needed to explore possible causes of these instabilities, closely related to the radiative heat transfer mode.

The third-order characteristic Eq. (38) based on the Rosseland approximation, on the other hand, yields only one positive root γ_1. The corresponding fluid and

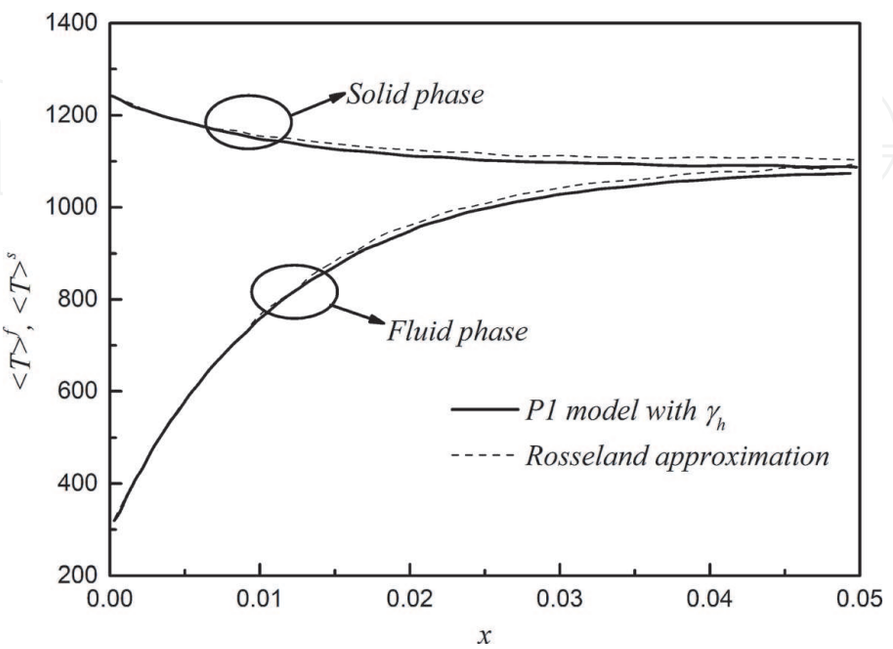

Figure 3.
Comparison of the temperature developments with the Rosseland approximation and P1 model.

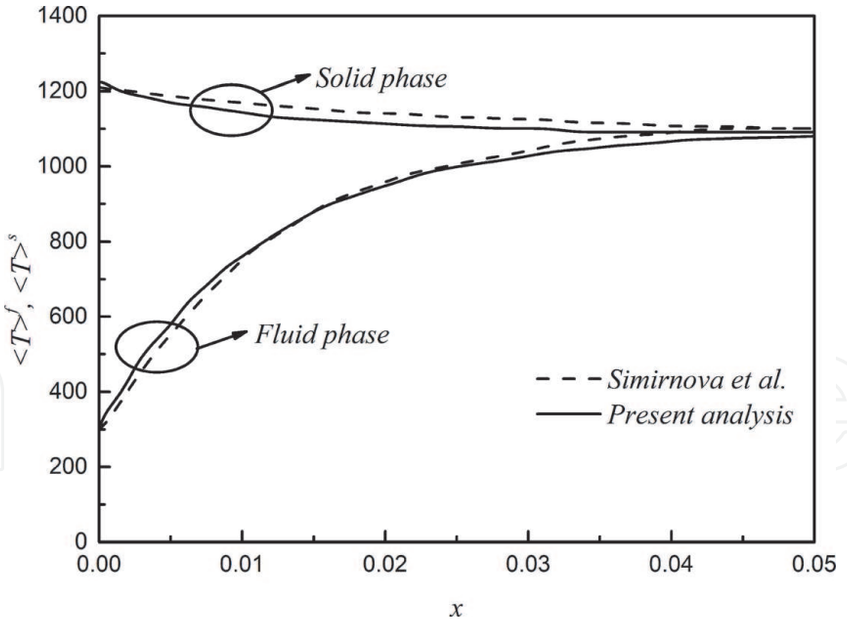

Figure 4.
Axial developments of the fluid and solid phase temperatures: comparison of the present analysis and FEM analysis.

solid temperature variations generated under the Rosseland approximation are compared with those based on the P1 model with the larger root γ_h. **Figure 3** shows that both sets of the temperature developments agree fairly well with each other. Thus, the Rosseland approximation for this case, despite its failure near the inlet boundary, is fairly accurate and may well be used for quick estimations and further analysis.

In **Figure 4**, the present analytic solutions are compared against the large-scale FEM numerical calculations based on COMSOL, reported by Smirnova et al. [23]. It should be mentioned that the direct numerical integrations of Eqs. (20)–(22) were also carried out using the finite volume method code, SAINTS [12]. As the convergence criteria, the residuals of all equations are less than 10^{-5}. It can be clearly seen that the air temperature increases as receiving heat from the monolithic receiver. Eventually, these two phases reach local thermal equilibrium near the exit. Both sets of solutions agree very well with each other, indicating the validity of the present local thermal non-equilibrium model.

5. Applications to silicon carbide ceramic foam volumetric receiver

In order to overcome the problems associated with thermal spots and flow instabilities, we would like to study fluid flow and heat transfer characteristics in silicon carbide ceramic foams based on the analytical expressions of pressure and temperature fields within a solar volumetric receiver. The performance of the receiver may be assessed in terms of the receiver efficiency η under equal pumping powerPP. Thus, the effects of the pore diameter d_m on the receiver efficiency η are presented in **Figure 5**, since d_m is a crucial geometry parameter affecting hydrodynamic and thermal characteristics of foam shown in Eqs. (23), (24) and (27). The pore diameter d_m is varied whereas the other parameters are fixed as follows:

$$\left\langle \rho_f \right\rangle_0^f = 1.2[\mathrm{kg/m^3}],\ \langle T\rangle_0^f = 300[\mathrm{K}](\langle p\rangle_0^f = 10^5[\mathrm{Pa}]),\ c_p = 1000[\mathrm{J/kgK}],$$
$$L = 0.03[m],\ I_0 = 10^6[\mathrm{W/m^2}],\ \xi = 0, h_{conv} = 0[\mathrm{W/m^2K}],\ k_s = 150[\mathrm{W/mK}],\ \varepsilon = 0.9.$$

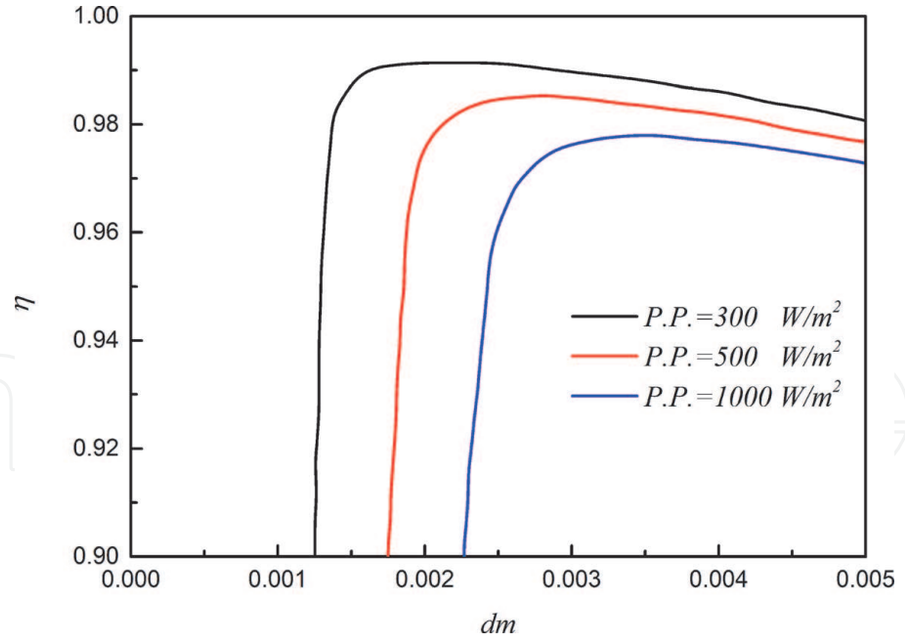

Figure 5.
Effects of the pore diameter on the receiver efficiency.

All other parameters are evaluated using Eqs. (17), (18) and from Eq. (23) to (28).

As shown in **Figure 5**, it is interesting to note that η suddenly increases at some critical value of d_m for a given value of PP, which means that the pore diameter d_m must be larger than this critical value to achieve high η. This finding is useful to design a volumetric receiver, and can be interpreted in what follows.

As indicated in Eq. (46), it can be easily deduced that $G \propto \sqrt{PP}$ for low PP and $G \propto \sqrt[3]{PP}$ for high PP, which results in that the amount of heat carried by the air, $G\left(T_{eq} - \langle T\rangle_0^f\right) \propto \sqrt{PP}$, increases drastically on increasing the pumping power PP from zero. Nevertheless, its rate of increase diminishes for the higher PP range, in which $G\left(T_{eq} - \langle T\rangle_0^f\right) \propto \sqrt[3]{PP}$. Moreover, it can also be concluded that the sharp rise in the receiver efficiency occurs around the transition from the Darcy to Forchheimer regime, namely,

$$\frac{\mu_0}{K}\left(\frac{T_{eq}}{\langle T\rangle_0^f}\right)^n G_{tr} \cong b{G_{tr}}^2 \tag{65}$$

or

$$G_{tr} \cong \left(\frac{\mu_0}{bK}\left(\frac{I_0 \cos\xi}{c_p\langle T\rangle_0^f}\right)^n\right)^{\frac{1}{1+n}} \tag{66}$$

since

$$\frac{T_{eq}}{\langle T\rangle_0^f} \cong \frac{c_p G_{tr}\langle T\rangle_0^f + I_0\cos\xi}{c_p G_{tr}\langle T\rangle_0^f} \cong \frac{I_0\cos\xi}{c_p G_{tr}\langle T\rangle_0^f} \tag{67}$$

Thus, Eq. (46) may be written for the case in which the sharp rise in η takes place as follows:

$$PP = \frac{G_{tr}}{\left(\langle\rho\rangle_0^f\right)^2}\left(2bG_{tr}{}^2\right)\left(\frac{T_{eq}}{\langle T\rangle_0^f}\right)^2 L \cong \frac{2bLG_{tr}{}^3}{\left(\langle\rho\rangle_0^f\right)^2}\left(\frac{I_0\cos\xi}{c_pG_{tr}\langle T\rangle_0^f}\right)^2$$
$$= \frac{2bL}{\left(\langle\rho\rangle_0^f\right)^2}\left(\frac{I_0\cos\xi}{c_p\langle T\rangle_0^f}\right)^2\left(\frac{\mu_0}{bK}\left(\frac{I_0\cos\xi}{c_p\langle T\rangle_0^f}\right)^n\right)^{\frac{1}{1+n}} \tag{68}$$

which, for given PP, gives the minimum value of the pore diameter d_{mtr}:

$$\frac{d_{mtr}}{L} = f(\varepsilon)\left(\frac{2}{\left(\langle\rho\rangle_0^f\right)^2 PP}\left(\frac{I_0\cos\xi}{c_p\langle T\rangle_0^f}\right)^3\right)^{\frac{1+n}{2+n}}\left(\frac{\mu_0}{\left(\frac{I_0\cos\xi}{c_p\langle T\rangle_0^f}\right)L}\right)^{\frac{1}{2+n}} \tag{69}$$

$$f(\varepsilon) = \left(\frac{(bd_m)^n}{K/d_m{}^2}\right)^{\frac{1}{2+n}} = \left(\frac{(12(1-\varepsilon))^n}{0.00073(1-\varepsilon)^{-0.224}\left(\frac{1.18}{1-e^{-(1-\varepsilon)/0.04}}\sqrt{\frac{1-\varepsilon}{3\pi}}\right)^{-1.11}}\right)^{\frac{1}{2+n}} \tag{70}$$

For PP = 300, 500 and 1000 W/m^2 studied here, Eq. (69) gives d_{mtr}= 0.0022, 0.0016 and 0.0010 m, respectively. It is consistent with what is observed in **Figure 5**, since an increase in d_m (i.e., decrease inβ) from d_{mtr} makes further penetration of the solar radiation possible. This works to keep the solid temperature at the inlet comparatively low such that heat loss to the ambient by radiation is suppressed. As a result, high receiver efficiency can be achieved. However, the increase in d_m on the other hand results in decreasing the volumetric heat transfer coefficient, as can be seen from Eq. (27). Too large d_m deteriorates interstitial heat transfer from the solid to air. Thus, as can be seen from the figure, the optimal size of d_m exits under the equal pumping power constraint.

In order to achieve local thermal equilibrium for the two phases within the receiver, the length of the receiver is assumed to be sufficiently long in the present study. In view of minimizing the required pumping power, however, it is noticeable that shorter length is better, as clearly seen from Eq. (46). Hence, a minimum length required to approach local thermal equilibrium may be chosen to design a receiver, which would guarantee both maximum receiver efficiency and minimum pumping power. Therefore, we may roughly set the optimal receiver length as

$$L = \frac{3}{\gamma\lambda} \tag{71}$$

such that

$$\frac{\langle T\rangle^f\big|_{x=L} - T_{eq}}{\langle T\rangle_0^f - T_{eq}} = \frac{\langle T\rangle^s|_{x=L} - T_{eq}}{\langle T\rangle_0^s - T_{eq}} = e^{-3} \cong 5\% \tag{72}$$

Eq. (71) together with Eq. (69) provides useful information for designing a volumetric solar receiver of silicon carbide ceramic foam.

6. Conclusions

For the first time, the complete set of analytical solutions, which fully considers the combined effects of turbulence, tortuosity, thermal dispersion, compressibility

on the convective, conductive and radiative heat transfer within a ceramic foam receiver, is presented based on the two-energy equation model of porous media. Both the Rosseland approximation and the P1 model are applied to account for the radiative heat transfer through the solar receiver, while the low Mach approximation is exploited to investigate the compressible flow through the receiver. Based on the P1 model, two positive roots were found from the characteristic equations of the fifth-order differential equation, indicating possible occurrence of hydrodynamic and thermal instabilities. However, it has been found that the Rosseland approximation for this case, despite its failure near the inlet boundary, is fairly accurate and may well be used for quick estimations and further analysis. Due to their advantages, such as high thermal conductivity and fluid mixing, silicon carbide ceramic foams are considered as a possible candidate for the receiver, which can overcome the problems associated with thermal spots and flow instabilities. The results show that the pore diameter must be larger than its critical value to achieve high receiver efficiency. As a result, there exists an optimal pore diameter for achieving the maximum receiver efficiency under the equal pumping power. The optimal pore diameter yielding the maximum receiver efficiency may be found around the critical value given by Eq. (71). A simple relation is derived for determining the length of the volumetric solar receivers of silicon carbide ceramic foam.

Conflict of interest

The authors declare no conflict of interest.

Nomenclature

A	surface area (m^2)
A_{int}	interfacial surface area between the fluid and solid (m^2)
b	inertial coefficient (1/m)
c	specific heat (J/kg K)
cp	specific heat at constant pressure (J/kg K)
d_m	pore diameter (m)
G	mass flux (kg/m^2 s)
h	specific enthalpy (J/kg)
h_v	volumetric heat transfer coefficient (W/m^3K)
I_0	intensity of radiation (W/m^2)
k	thermal conductivity (W/m K)
K	permeability (m^2)
L	receiver length (m)
n_j	normal unit vector from the fluid side to solid side (−)
PP	pumping power per unit frontal area (W/m^2)
Pr	Prandtl number (−)
q	heat flux (W/m^2)
R	gas constant (J/kg K)
T	temperature (K)
u_i	velocity vector (m/s)
V	representative elementary volume (m^3)
x_i	Cartesian coordinates (m)
x	axial coordinate (m)

β	mean extinction coefficient (1/m)
γ	dimensionless parameter (−)
ε	porosity (−)
ε^*	effective porosity (−)
ξ	incidence angle (rad)
η	receiver efficiency (−)
λ	characteristic coefficient (1/m)
μ	viscosity (Pa s)
ν	kinematic viscosity (m^2/s)
ρ	density (kg/m^2)
σ	Stephan-Boltzmann constant (W/m^2K^4)
κ	absorption coefficient (1/m)
τ_{ij}	stress tensor (Pa)

Special symbols

$\tilde{\varphi}$	deviation from intrinsic average
$\langle\phi\rangle$	Darcian average
$\langle\phi\rangle^{f,s}$	intrinsic average

Subscripts and superscripts

dis	dispersion
eq	equilibrium
f	fluid
s	solid
stag	stagnation
0	reference

Author details

Chen Yang[1], Huijin Xu[2*] and Akira Nakayama[3]

1 College of Chemical Engineering, Fuzhou University, China

2 China-UK Low Carbon College, Shanghai Jiao Tong University, China

3 Faculty of Engineering, Shizuoka University, Japan

*Address all correspondence to: xuhuijin@sjtu.edu.cn

References

[1] Fend T. High porosity materials as volumetric receivers for solar energetics. Optica Applicata. 2010; **40**(2):271-284

[2] Alexoprrroulos S, Hoffschmidt B. Solar tower power plant in Germany and future perspectives of the development of the technology in Greece and Cyprus. Renewable Energy. 2010;**35**:1352-1356

[3] Pitz-Paal R, Hoffschmidt B, Bohmer M, Becker M. Experimental and numerical evaluation of the performance and flow stability of different types of open volumetric absorbers under non-homogeneous irradiation. Solar Energy. 1997;**60**:135-150

[4] Becker M, Fend T, Hoffschmidt B, Pitz-Paal R, Reutter O, Stamatov V, et al. Theoretical and numerical investigation of flow stability in porous materials applied as volumetric solar receiver. Solar Energy. 2006;**80**: 1241-1248

[5] Fend T, Hoffschmidt B, Pitz-Paal R, Reutter O. Porous materials as open volumetric solar receivers: Experimental determination of thermophysical and heat transfer properties. Energy. 2004; **29**:823-833

[6] Bai F. One dimensional thermal analysis of silicon carbide ceramic foam used for solar air receiver. International Journal of Thermal Sciences. 2010;**49**: 2400-2404

[7] Sano Y, Iwase S, Nakayama A. A local thermal non-equilibrium analysis of silicon carbide ceramic foam as a solar volumetric receiver. Journal of Solar Energy Engineering, Transactions of the ASME. 2012;**134**(2):021006

[8] Wu Z, Caliot C, Flamant G, Wang Z. Numerical simulation of convective heat transfer between air flow and ceramic foams to optimize volumetric solar air receiver performances. International Journal of Heat and Mass Transfer. 2011; **54**:1527-1537

[9] Yang C, Nakayama A. A synthesis of tortuosity and dispersion in effective thermal conductivity of porous media. International Journal of Heat and Mass Transfer. 2010;**53**(15–16):3222-3230

[10] Neuman SP. Theoretical derivation of Darcy's law. Acta Mechanica. 1977;**25**: 153-170

[11] Cheng P. Heat transfer in geothermal systems. Advances in Heat Transfer. 1978;**14**:1-105

[12] Nakayama A. PC-Aided Numerical Heat Transfer and Convective Flow. CRC Press; 1995. pp. 49-50, 103-115

[13] Quintard M, Whitaker S. One and two equation models for transient diffusion processes in two-phase systems. Advances in Heat Transfer. 1993;**23**:369-465

[14] Nakayama A, Kuwahara F, Kodama Y. An equation for thermal dispersion flux transport and its mathematical modelling for heat and fluid flow in a porous medium. Journal of Fluid Mechanics. 2006;**563**:81-96

[15] Calmidi VV, Mahajan RL. The effective thermal conductivity of high porosity fibrous metal foams. Transactions of the ASME, Journal of Heat Transfer. 1999;**121**:466-471

[16] Calmidi VV, Mahajan RL. Forced convection in high porosity metal foams. Transactions of the ASME, Journal of Heat Transfer. 2000;**122**:557-565

[17] Dukhan N. Correlations for the pressure drop for flow through metal foam. Experiments in Fluids. 2006;**41**: 665-672

[18] Kuwahara F, Yang C, Ando K, Nakayama A. Exact solutions for a thermal non-equilibrium model of fluid saturated porous media based on an effective porosity. Transactions of the ASME, Journal of Heat Transfer. 2011; **133**(11):112602

[19] Yang C, Ando K, Nakayama A. A local thermal non-equilibrium analysis of fully developed forced convective flow in a tube filled with a porous medium. Transport in Porous Media. 2011;**89**:237-249

[20] Yang C, Kuwahara F, Liu W, Nakayama A. Thermal non-equilibrium forced convective flow in an annulus filled with a porous medium. The Open Transport Phenomena Journal. 2011;**3**: 31-39

[21] Kamiuto K, Miyoshi Y, Kinoshita I, Hasegawa S. Conduction in optically thick ceramic porous media: Radiative heat transfer for the case of cordierite foam. Transactions of the JSME, Series B. 1983;**49**:2147-2153

[22] Nakayama A, Kuwahara F. A general macroscopic turbulence model for flows in packed beds, channels, pipes and rod bundles. ASME Transactions Journal of Fluids Engineering. 2008;**130**(10):101205

[23] Smirnova O, Fend T, Peter S, Schollgen D. Homogeneous and inhomogeneous model for flow and heat transfer in porous materials as high temperature solar air receiver. In: Proceedings of the COMSOL Conference; Paris. 2010. pp. 17-19

[24] Agrafiotis C, Mavroidis I, Konstandopoulos AG, Hoffschmidt B, Stobbe P, Romero M, et al. Evaluation of porous silicon carbide monolithic honeycombs as volumetric receivers/ collectors of concentrated solar radiation. Solar Energy Materials and Solar Cells. 2007;**91**:474-488